INSTITUTE OF PHYSICS PUBLISHING MEASUREMENT SCIENCE AND TECHNOLOGY

Meas. Sci. Technol. **17** (2006) N81–N86 doi:10.1088/0957-0233/17/12/N02

DESIGN NOTE

Using the fringing fields of a hemispherical spectrograph to improve its energy resolution

T J M Zouros[1,2], Omer Sise[3], Melike Ulu[3] and Mevlut Dogan[3]

[1] Department of Physics, University of Crete, PO Box 2208, 71003 Heraklion, Crete, Greece
[2] Institute of Electronic Structure and Laser, PO Box 1527, 71110 Heraklion, Crete, Greece
[3] Department of Physics, Science and Arts Faculty, Afyon Kocatepe University, 03200 Afyonkarahisar, Turkey

E-mail: tzouros@physics.uoc.gr

Received 14 July 2006, in final form 13 September 2006
Published 14 November 2006
Online at stacks.iop.org/MST/17/N81

Abstract
The energy resolution of a hemispherical deflector analyser (HDA) can be substantially improved by using its entry fringing fields advantageously, rather than trying to eliminate them—the traditional approach. The intrinsic lensing properties of these fringing fields, as shown in simulations, are able to not only restore, but even improve first-order focusing at the 180° deflection plane in a controlled way, without the use of any additional field correction electrodes. This is accomplished by changing the entry radius R_0 and bias $\widetilde{V}(R_0)$ from their conventional values of $R_0 = \overline{R}$, the mean radius $\overline{R} = (R_1 + R_2)/2$ and $\widetilde{V}(R_0) = 0$ to new values $R_0 > \overline{R}$ with $\widetilde{V}(R_0) < 0$ or $R_0 < \overline{R}$ with $\widetilde{V}(R_0) > 0$. An HDA with $\overline{R} = 101.6$ mm, $\Delta R = R_2 - R_1 = 58.4$ mm and maximum entry angle $\alpha_{\max} = 2°$ demonstrates the impressive resolution gains that can be attained, 34 for a point entry ($\Delta r_0 = 0$) and 4.2 for an aperture diameter of $\Delta r_0 = 1$ mm, over corresponding conventional entry conditions.

Keywords: energy resolution, hemispherical deflector analysers, fringing field correctors, high resolution electron spectroscopy, electron optics, SIMION

(Some figures in this article are in colour only in the electronic version)

1. Introduction

Strong fringing fields at the entry and exit of HDAs with large interradial electrode separations $\Delta R(\equiv R_2 - R_1)$ are known to be particularly deleterious to 180° first-order focusing conditions, one of the central advantages of the ideal-field ($1/r^2$) HDA [1]. The exit radial width Δr_π in such an HDA is seen in figure 1(*b*) to become particularly defocused in figure 1(*e*) leading to a corresponding drastic deterioration in its energy resolution. Thus, various fringing field correction schemes [2] have been traditionally applied to reduce this defocusing and restore ideal field behaviour.

Recently, Benis and Zouros [3] showed in simulation that the energy resolution of an HDA with strong fringing fields could be improved *without* additional corrector electrodes. This was accomplished by utilizing novel HDA entry conditions, quite different from the conventional conditions traditionally used with $R_0 = \overline{R}$ and $\widetilde{V}_0 \equiv \widetilde{V}(R_0) = 0$ illustrated in figures 1(*b*) and (*e*). Specifically, they found that for particular combinations of R_0-values *smaller* than the mean radius $\overline{R}$ and *positive* entry bias $\widetilde{V}_0 > 0$, improved

 © 2006 IOP Publishing Ltd Printed in the UK

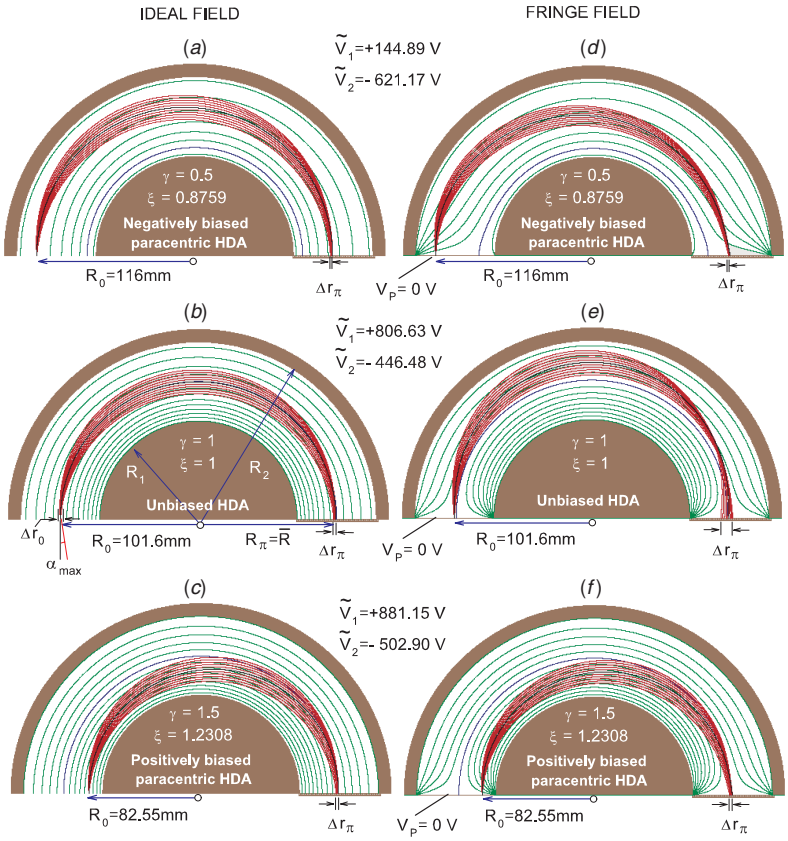

Figure 1. Schematic of ideal $1/r^2$ ((*a*)–(*c*)) and fringing ((*d*)–(*f*)) field HDAs with $R_1 = 72.4$ mm and $R_2 = 130.8$ mm [5] simulated by SIMION and used to calculate line shapes for electron trajectories in the equatorial $z = 0$ XY dispersion plane. (*a*) and (*d*) Negative bias paracentric entry with $R_0 = 116$ mm and $\gamma = 0.5$; (*b*) and (*e*) conventional entry with $R_0 = \overline{R} = 101.6$ mm and $\gamma = 1$ (zero bias); (*c*) and (*f*) positive bias paracentric entry with $R_0 = 82.55$ mm and $\gamma = 1.5$. The three ideal field entries (*a*)–(*c*) and fringing field paracentric entries (*d*) and (*f*) result in first-order focusing at the PSD, while fringing field conventional entry (*e*) results in an unfocused image with a much larger base width. Green lines mark equipotentials every 100 V. The blue line marks the equipotential $\widetilde{V} = 0$. The central rays having $\alpha = 0^\circ$ are marked in black. The HDA base plate—here simulated by a grid biased at $V_p = 0$ V—gives rise to the strong fringing fields in cases (*d*)–(*f*). The size of the beam entry width (object) Δr_0 centred around R_0, here taken to be a point source $\Delta r_0 = 0$, is also shown. Line shapes resulting for cases (*a*)–(*c*) are shown in figure 2, and for (*d*)–(*f*) in figure 3. Numerical results are listed in table 1.

focusing could be recovered with a corresponding substantial improvement in HDA energy resolution (see figure 1(*f*)). This type of HDA is referred to here as a positively *biased paracentric* HDA. Such a *real* (not simulated) positively biased paracentric HDA, utilizing a four element zoom lens and position sensitive detector (PSD), has been successfully applied to zero-degree Auger projectile electron spectroscopy in energetic ion–atom collisions [4, 5] with excellent resolution ($\lesssim$0.1%). While this resolution improvement is still under investigation, it has recently been shown that *no* such improvement is found for the *ideal*-field positively biased paracentric HDA [6], which in fact has a slightly worse resolution than the ideal-field conventional HDA [7]. Thus, clearly, the strong fringing fields must be necessarily involved.

Here, we provide a more in depth investigation of paracentric entry conditions. We show, via electron optics simulations using SIMION [8], that the energy resolution of an HDA is not only improved for the particular combination of $R_0 < \overline{R}$ and $\widetilde{V}_0 > 0$, already reported in [3] and shown in case (*f*) of figure 1, but also for other combinations of values with R_0 *larger* than $\overline{R}$ ($R_0 > \overline{R}$) having *negative* entry bias $\widetilde{V}_0 < 0$, as illustrated in figure 1(*d*). We have performed a systematic search for the optimal values of R_0 and $\widetilde{V}_0$ minimizing Δr_π over the entire range $R_1 < R_0 < R_2$ for both positive and negative values of $\widetilde{V}_0$, thus extending the study of [3] to include also negative bias. The newly discovered negative bias paracentric entry conditions reported here are found to lead to substantially better resolution than those of the older positive bias case. These results should be generic for any HDA with the optimal combinations of R_0 and $\widetilde{V}_0$ readily determined through electron optics simulations as described next.

2. Simulations and results

SIMION [8] trajectory calculations were performed for monoenergetic electrons ($q = -|e|$) with pass energy E_0 and electrode potentials $\widetilde{V}_i \equiv \widetilde{V}(R_i)$ ($i = 1, 2$) given by

$$q\widetilde{V}_i = E_0\left[1 - \gamma\left(\frac{R_0}{R_\pi}\right)\left(\frac{R_0 + R_\pi}{R_i} - 1\right)\right] \quad (i = 1, 2). \tag{1}$$

In an *ideal* field HDA, these voltages, as discussed in detail in [6, 9], allow the central ray (entering at R_0 with energy E_0

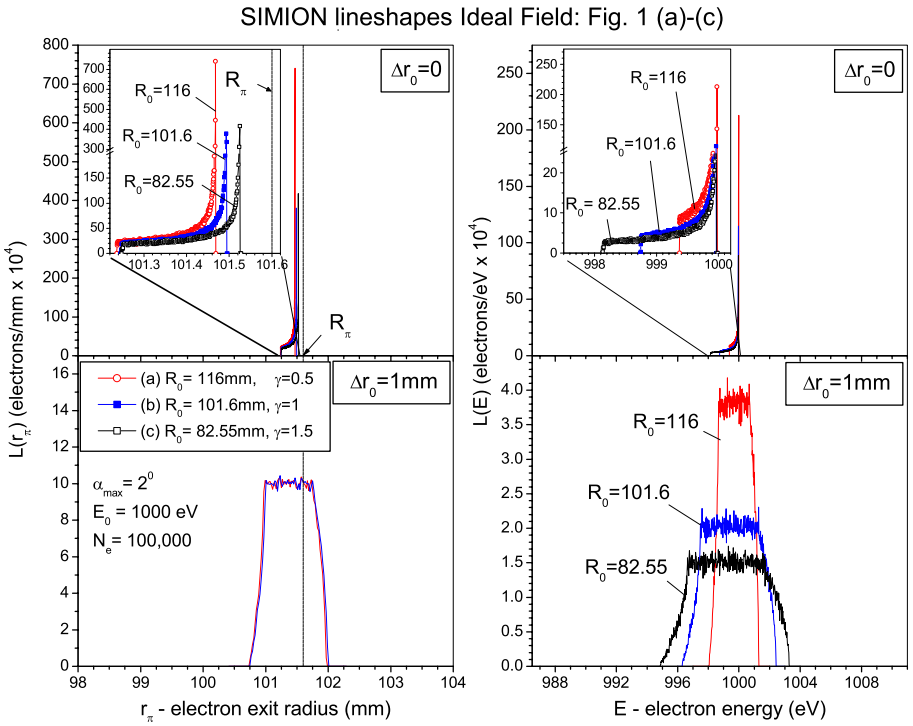

Figure 2. SIMION line shapes $L(r_\pi)$ (left) and $L(E)$ (right) with respect to exit radial position r_π and electron energy E, respectively, are shown for the *ideal* field HDA cases of figures 1 (*a*)–(*c*). Results are for a pass energy $E_0 = 1000$ eV, random entry angle α with $|\alpha| \leqslant \alpha_{\max} = 2^\circ$ for point source (aperture diameter $\Delta r_0 = 0$—top panels) and extended source ($\Delta r_0 = 1.0$ mm—bottom panels). Different bin sizes have been used as necessary. Line shapes have been normalized so that $\int L(r_\pi)\,\mathrm{d}r_\pi = \int L(E)\,\mathrm{d}E = 100\,000$ electrons. Details can be seen more clearly in the blow-ups of the indicated regions. Numerical values are given in table 1. For all three entries (*a*), (*b*) and (*c*) first-order focusing is achieved yielding comparable values of Δr_π (left panels). Dispersion lengths, however, increasing with R_0, yield correspondingly decreasing energy widths ΔE_B (right panels). The negative bias paracentric entry having the largest R_0 ($R_0 = 116$ mm) is seen to have the smallest ΔE_B (best resolution).

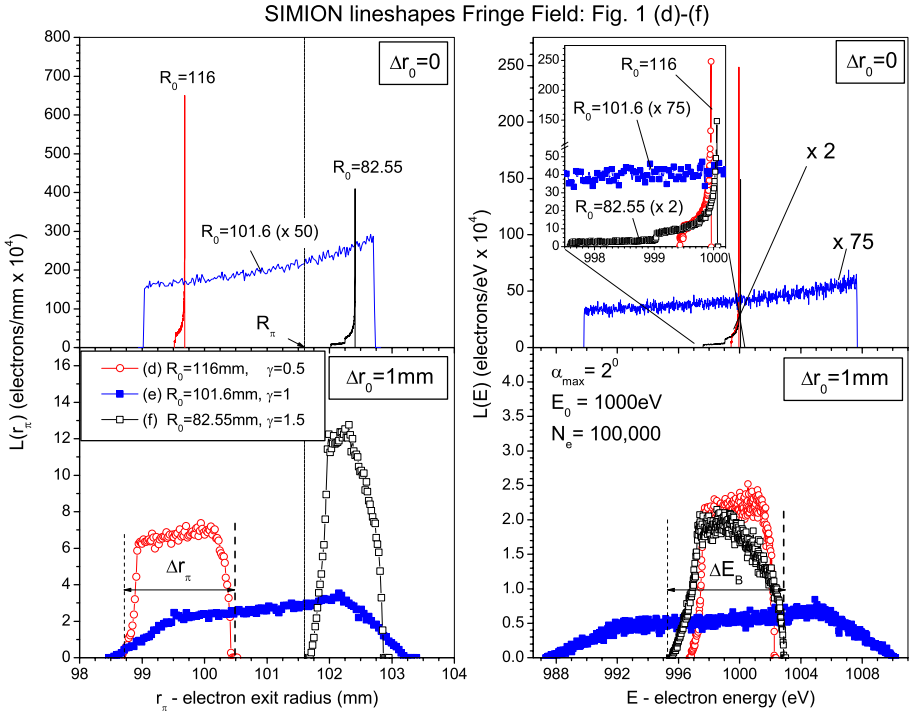

Figure 3. Same as for figure 2, but for the *fringing* field HDA cases of figures 1 (*d*)–(*f*). Conventional entry with $R_0 = 101.6$ mm (case (*e*) in figure 1) is seen to have a very defocused image at the PSD with a corresponding degradation of energy resolution. Paracentric entries with $R_0 = 116$ mm and $R_0 = 82.55$ mm (cases (*d*) and (*f*) in figure 1), however, are seen to have comparable if not better, radial widths Δr_π (left panels) and base energy widths ΔE_B (right panels) compared to the corresponding ideal field cases figure 2 (*a*) and (*c*), respectively. Overall, the negatively biased entry using $R_0 = 116$ mm (red line) is seen to have the best resolution, particularly at small values of Δr_0.

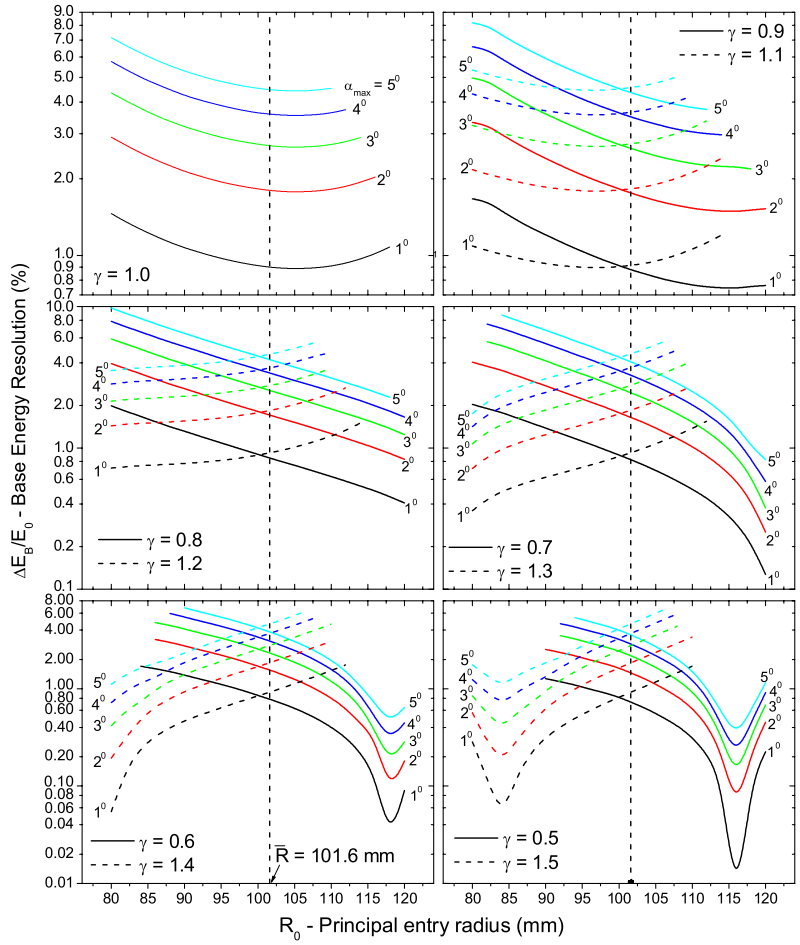

Figure 4. Base energy resolution $\Delta E_B/E_0$ plotted as a function of R_0 for different values of maximum entry angle $\alpha_{max} = 1°$–$5°$. Lines: $\gamma > 1$ (dashed) and $\gamma \leqslant 1$ (continuous). Resolution minima occur near $R_0 = 82.55$ mm with $\gamma = 1.5$ and $R_0 = 116$ mm with $\gamma = 0.5$.

and angle $\alpha = 0°$) to exit at R_π. It makes sense to choose $R_\pi = \overline{R}$, as done here, so that placing the centre of the PSD at $\overline{R}$ automatically also sets it at the centre of the energy acceptance window of the HDA tuned to pass energy E_0. The parameter γ in equation (1) conveniently controls the voltages V_i via a single parameter. For an *ideal* potential γ sets the value of the entry bias $\widetilde{V}_0 \equiv \widetilde{V}(R_0)$ via the relation [6]

$$q\widetilde{V}_0 = (1-\gamma)E_0, \tag{2}$$

and is therefore known as the biasing parameter. In the case of fringing field HDAs, $\widetilde{V}_0$ is only used as a nominal setting (a kind of label). It is also convenient to define the paracentricity $\xi \equiv \overline{R}/R_0$ of an HDA. Thus, a conventional entry HDA will have $\xi = 1$ ($R_0 = \overline{R}$) and $\gamma = 1$ ($\widetilde{V}_0 = 0$), while a paracentric entry HDA with $\xi < 1$ ($\xi > 1$) or equivalently $R_0 > \overline{R}$ ($R_0 < \overline{R}$) is biased correspondingly negatively $\gamma < 1$ (positively $\gamma > 1$). We have found the best resolution to be attained for the paracentric cases with $\xi = 0.8759$ and $\gamma = 0.5$ and $\xi = 1.2308$ and $\gamma = 1.5$. In figure 1, focusing conditions for both conventional entry (*b*) and (*e*) and optimum paracentric entries (*a*), (*d*) and (*c*), (*f*) are illustrated. The corresponding line shapes $L(r_\pi)$ and $L(E)$ are compared in figures 2 and 3 for an HDA tuned to the pass energy E_0.

The line shape simulations shown in figures 2 and 3 were performed using a Monte Carlo type approach with the entry angle α randomly sampled over the range $|\alpha| \leqslant \alpha_{max} = 2°$. 100 000 monoenergetic electrons of energy $E_0 = 1000$ eV were emitted from points within the entry aperture diameter Δr_0 centred on R_0. The grid density used in the SIMION simulation was $\lambda = 10$ gu mm^{-1} (gu = grid units) with the HDA optimized for highest accuracy as discussed in detail in [9]. The determined exit radial positions r_π were converted to energies E using central rays of known energy and a quadratic energy calibration procedure. The extracted radial widths Δr_π and corresponding base energy resolutions ΔE_B are listed in table 1. While Δr_π provides direct information on the focusing properties of the HDA, ΔE_B also includes the effect of energy dispersion. Thus, for the same Δr_π, the HDA with the largest dispersion length $D_0 \equiv R_0 + R_\pi$ can be expected to have the smallest ΔE_B.

In figure 4, the results of our search for the values of R_0 and γ that minimize Δr_π and ΔE_B are shown for point source ($\Delta r_0 = 0$) emission. The resulting base resolution $\Delta E_B/E_0$ is plotted for different maximum entry angles $\alpha_{max} = 1°$–$5°$. The best energy resolution as already mentioned is attained near $R_0 = 82.55$ mm ($\xi = 1.2308$) for $\gamma = 1.5$ and $R_0 = 116$ mm ($\xi = 0.8759$) for $\gamma = 0.5$. The optimal values of R_0 and γ remain practically unchanged for small values of Δr_0 even though Δr_π and $\Delta E_B/E_0$ can change substantially.

Table 1. Detailed numerical results for simulated electron trajectories corresponding to HDA cases figures 1 (*a*)–(*f*), whose line shapes appear in figures 2 and 3 for pass energy $E_0 = 1000$ eV and $\alpha_{max} = 2^\circ$. In the case of the ideal field, theoretical calculations can also be performed and are compared to simulations. Central ray ($\alpha = 0$) exit radius r_π, maximal exit radial widths Δr_π and base energy widths ΔE_B are listed for ideal and fringing fields for both point ($\Delta r_0 = 0$) and extended sources ($\Delta r_0 = 1$ mm). Ideal potential $\widetilde{V}(r) = -k/r + c$ is simulated in SIMION by a spherical capacitor (SC) [9]. Constants k and c are determined from the electrode voltages $\widetilde{V}_1$ and $\widetilde{V}_2$ [6, 9] and are used for the ideal field theoretical calculations of r_π [6]. In this case, simulation and theory are seen to be in excellent agreement [9].

		HDA parameters									Electron trajectory results			
		Independent		Dependent							$\Delta r_0 = 0$ mm		$\Delta r_0 = 1$ mm	
Figure 1 #	Calculation	R_0 (mm)	γ	ξ	$\widetilde{V}_0^d$ (V)	$\widetilde{V}_1$ (V)	$\widetilde{V}_2$ (V)	k (V mm)[b]	c (V)[b]	Central ray r_π (mm)	Δr_π (mm)	ΔE_B (eV)	Δr_π (mm)	ΔE_B (eV)
Ideal field: spherical capacitor (SIMION parameters: $\lambda = 10$ gu mm^{-1}, $R_1 = 724$ gu, $R_2 = 1307$ gu [9])														
(*a*)	SIMION[a]	116.0	0.5	0.8759	−499.9925	144.8862	−621.1683	–	–	101.5	0.231	0.609	1.23	3.24
	Theory[c]	116.0	0.5	0.8759	−500	144.8862	−621.1683	−124 220	−1571	101.6	0.232	0.609	1.23	3.23
(*b*)	SIMION[a]	101.6	1	1	0.0936	806.6298	−446.4832	–	–	101.5	0.247	1.22	1.25	6.14
	Theory[c]	101.6	1	1	0	806.6298	−446.4832	−203 200	−2000	101.6	0.247	1.22	1.25	6.14
(*c*)	SIMION[a]	82.55	1.5	1.231	+500.2681	881.1507	−502.9028	–	–	101.5	0.277	1.84	1.28	8.46
	Theory[c]	82.55	1.5	1.231	+500	881.1507	−502.9028	−224 433	−2219	101.6	0.276	1.83	1.27	8.44
Fringe field: hemispherical deflector analyser (SIMION parameters: $\lambda = 10$ gu mm^{-1}, $R_1 = 724$ gu, $R_2 = 1307$ gu [9])														
(*d*)	SIMION[a]	116.0	0.5	0.8759	–	144.8862	−621.1683	–	–	99.68	0.168	0.525	1.75	5.45
(*e*)	SIMION[a]	101.6	1	1	–	806.6298	−446.4832	–	–	101.1	3.69	17.9	4.70	22.8
(*f*)	SIMION[a]	82.55	1.5	1.231	–	881.1507	−502.9028	–	–	102.4	0.387	2.46	1.15	7.27

[a] High accuracy calculations using a heavy electron mass $m = 10^{12} m_e$ to reduce relativistic effects [9].
[b] Defined for ideal potential (SC) only.
[c] Theory: non-relativistic (equation (99) of [6]).
[d] Ideal field (SC) only—for fringe field (HDA) electrons are launched from the entry grid at 0 V.

3. Discussion

Of central importance to this presentation is the discovery of the negative paracentric entry condition and its large resolution gain in the fringing field case (figure 1(*d*)) over that of the corresponding conventional entry ($R_0 = \overline{R}$ and $\widetilde{V}_0 = 0$) resolution (figure 1(*e*)). As shown in figure 3 and table 1, a gain factor of about 34 (= 17.9/0.525) is found for point source ($\Delta r_0 = 0$) emission, with a somewhat reduced gain of about 4.2 (= 22.8/5.45) for a more realistic entry aperture diameter of $\Delta r_0 = 1$ mm. For a point source, $\Delta r_\pi = 0.168$ mm is also smaller than the corresponding *ideal* field negative bias paracentric case with $\Delta r_\pi = 0.231$ mm, clearly showing that first-order focusing has even been *improved* in the case of the fringing field. For an extended source, however, the opposite is true, the negative bias paracentric HDA in the fringing field case has $\Delta r_\pi = 1.75$ mm is larger than $\Delta r_\pi = 1.23$ mm, the corresponding ideal field case. Similarly, the same holds true for the energy resolution.

For the positive bias paracentric HDA, the fringing field $\Delta r_\pi = 0.387$ mm is seen to be a bit larger than the corresponding ideal field case with $\Delta r_\pi = 0.276$ mm for point source. This reverses itself, however, for an extended source of $\Delta r_0 = 1$ mm, with the fringing field positive bias paracentric HDA having $\Delta r_\pi = 1.15$ mm, seen now to be somewhat *smaller* than the corresponding ideal field case with $\Delta r_\pi = 1.27$ mm and similarly for the energy resolution.

Overall, for the present parameter values, the best resolution seems to be attainable by the negatively biased paracentric HDA in both ideal and fringing field cases as well as for both point and extended sources. The best ultimate resolution will of course depend on the specific values of ΔR, R_0, γ, $\alpha_{\max}$ and Δr_0 [10]. Its detailed dependence on these parameters needs to be fully investigated. Presently, this can only be done in simulation.

The good resolution properties of the positive bias paracentric entry HDA have already been demonstrated in the laboratory [4, 5, 10]. However, the newly discovered negative bias paracentric entry conditions, reported here for the first time, have only been verified in simulations so far. An HDA that will be able to test these predictions in the laboratory is presently under design.

4. Conclusions

In conclusion, we have shown that there also exists a negative bias paracentric entry with $R_0 > \overline{R}$ and $\widetilde{V}_0 < 0$, with an even larger resolution gain than that of the positive bias paracentric entry HDA reported in [3]. For both negative and positive paracentric entries, the large improvement in energy resolution is particularly newsworthy as it is conveniently attained without the use of any type of additional fringing field correction electrodes, but simply by taking advantage of the strong intrinsic lensing effects of the *existing* HDA fringing fields. Clearly, this should reduce both the cost of construction and the complexity of using such an HDA. Thus, paracentric HDAs should be of great practical interest to all high resolution electron spectroscopy applications in general, but in particular to those delivering high throughput via the use of a PSD. In such an HDA, strong fringing fields are naturally present due to the much larger interradial electrode separations required to accommodate the PSDs and the use of corrector electrodes, which reduce transmission, is particularly problematic. It is our hope that these results will stimulate further interest in the construction and testing of such HDAs.

Acknowledgments

We acknowledge partial support from the Greek Ministry of Development (GSRT Project No GR-11/03), ELKE-University of Crete travel grant, the State Planning Organization in Turkey (grant 2002K120110) and the Scientific Research Project Commission of Afyon Kocatepe University (grant 031-FENED-07).

References

[1] Purcell E M 1938 *Phys. Rev.* **54** 818
[2] Sagara T, Boesten L, Nishida S and Okada K 2000 *Rev. Sci. Instrum.* **71** 4201
[3] Benis E P and Zouros T J M 2000 *Nucl. Instrum. Methods Phys. Res.* A **440** 462
[4] Benis E P *et al* 1998 *Nucl. Instrum. Methods Phys. Res.* B **146** 120
[5] Benis E P, Zouros T J M, Gorczyca T W, González A D and Richard P 2004 *Phys. Rev.* A **69** 052718
[6] Zouros T J M and Benis E P 2002 *J. Electron Spectrosc. Relat. Phenom.* **125** 221
Zouros T J M and Benis E P 2005 *J. Electron Spectrosc. Relat. Phenom.* **142** 175
[7] Zouros T J M 2006 *J. Electron Spectrosc. Relat. Phenom.* **152** 67
Zouros T J M 2006 *J. Electron Spectrosc. Relat. Phenom.* **153** 102–7
[8] Dahl D A 1996 *SIMION 3D v6.0* Idaho National Engineering Laboratory, Idaho Falls
[9] Zouros T J M, Sise O, Spiegelhalder F M and Manura D J 2006 *Int. J. Mass Spectr.* at press (http://dx.doi.org/10.1016/j.ijms.2006.08.005)
See also http://www.simion.com/tools/sc
[10] Zouros T J M and Benis E P 2005 *Appl. Phys. Lett.* **86** 094105